Monoenergetic photon-induced fission cross-section ratio measurements for ^{235}U, ^{238}U, and ^{239}Pu from 9.0 to 17.0 MeV

Krishichayan,[1,2,*] S. W. Finch,[1,2] C. R. Howell,[1,2] A. P. Tonchev,[3] and W. Tornow[1,2]

[1]*Triangle Universities Nuclear Laboratory, Durham, North Carolina, 27708, USA*

[2]*Department of Physics, Duke University, Durham North Carolina, 27708, USA*

[3]*Nuclear and Chemical Sciences Division, Lawrence Livermore National Laboratory, Livermore, California 94550, USA*

(Received 19 April 2018; revised manuscript received 13 June 2018; published 13 July 2018)

Background: High-accuracy data are needed to advance microscopic descriptions of the nuclear fission process, to improve the predictive precision of phenomenological models, and for applications in nuclear energy and homeland security.

Purpose: The main goal of this work is to provide high-accuracy cross-section data for photofission of ^{235}U, ^{238}U, and ^{239}Pu in the energy range from the fission threshold to the high-energy tail of the giant dipole resonance. These new data should contribute significantly to the reduction of the systematic uncertainty in evaluated photofission cross-section databases.

Method: Cross-section ratios for photofission of the "big three" actinide nuclei were measured using a quasimonoenergetic photon beam and dual-fission chambers. The measurements were performed at the HIγS facility using a photon beam produced from Compton backscattering of free-electron laser light. The dual-fission chamber enabled simultaneous counting of fission events from two targets. This method allows for cross-section ratio measurements with very small systematic errors. The largest source of systematic error in the determination of the cross-section ratios is the uncertainty in the ratio of the target thicknesses.

Results: We report photon-induced fission cross-section ratios for $\sigma[^{235}\mathrm{U}(\gamma,f)/^{238}\mathrm{U}(\gamma,f)]$, $\sigma[^{235}\mathrm{U}(\gamma,f)/^{239}\mathrm{Pu}(\gamma,f)]$, and $\sigma[^{238}\mathrm{U}(\gamma,f)/^{239}\mathrm{Pu}(\gamma,f)]$ at photon energies from 9.0–17.0 MeV. More than 20 data points were measured for each ratio, and the systematic uncertainties are less than 2%.

Conclusion: The present photofission cross-section ratio data sets are compared to ratios computed from previous measurements, to the corresponding neutron-induced fission cross-section ratios, and to ratios computed from evaluated databases. The data obtained in this work for $\sigma[^{235}\mathrm{U}(\gamma,f)/^{238}\mathrm{U}(\gamma,f)]$ are consistent with the existing data, while for $\sigma[^{235}\mathrm{U}(\gamma,f)/^{239}\mathrm{Pu}(\gamma,f)]$ and $\sigma[^{238}\mathrm{U}(\gamma,f)/^{239}\mathrm{Pu}(\gamma,f)]$ the present data are systematically lower.

DOI: 10.1103/PhysRevC.98.014608

I. INTRODUCTION

Since its discovery in 1939 [1,2] nuclear fission has served as a rich laboratory for nuclear structure studies that involve both single-particle and collective motion under conditions of violent rearrangements of the nucleons. High-accuracy data are needed to advance microscopic descriptions of phenomena associated with fission and to improve the predictive power of phenomenological models. While there has been much progress in understanding the fission process over the past 78 years, a completely satisfactory theory of nuclear fission does not exist. A complete and quantitatively accurate microscopic and/or macroscopic fission model would significantly impact a number of applications in areas of nuclear stockpile stewardship, nuclear nonproliferation technologies, and nuclear energy.

Precise data for photon-induced nuclear fission are important in a variety of research and development areas, e.g., basic nuclear physics, activation analysis of materials, remote detection of nuclear materials, nuclear forensics, production of medical isotopes, and physics and technology of fission reactors [3–8].

An improved understanding of fission cross-section data would also impact the detection and identification of special nuclear materials (SNMs) through active and passive interrogation techniques [9], as these methods rely on detecting γ rays and neutrons emitted by the fissioning nuclei. The appeal of using photofission in this application is enhanced by the recent demonstration of a novel laser-wakefield accelerator-based γ-ray source [10,11], which raises the prospect of a portable, linearly polarized γ-ray source for active interrogation.

A vast majority of the existing fission data come from neutron-induced fission [12]. Depending on the incident energy a neutron can bring different amounts of angular momentum into the system, changing how the nucleus evolves through the fission barrier and ultimately affecting the resulting observables. This means that neutron-induced fission data are a combination of multiple modes of the already complex fission reaction, making consistent interpretations of observables difficult.

On the other hand, the use of an electromagnetic probe in fission studies, such as real photons, simplifies the interpretation

*krishi@tunl.duke.edu; krishichayan@gmail.com

of data by offering the advantage of a well-known interaction with strict angular-momentum selection rules. Photon absorption at low energies (below about 100 MeV) is predominantly $E1$ absorption and to a smaller extent $M1$ and $E2$ absorptions. Another special feature of photon probes, as opposed to hadronic probes, is the absence of binding energy of the projectile with the target nucleus to form the compound nuclear system that fissions. That is, for photofission the excitation energy of the precursor compound nucleus corresponds to the energy of the incident photon. In addition, because the photon is electrically neutral, there is no Coulomb barrier in the entrance channel. These features give rise to the unique possibility of studying nuclear fission at any excitation energy above or below the fission barrier, e.g., sub-barrier fission [13].

II. PHOTOINDUCED FISSION OF ^{235}U, ^{238}U, and ^{239}Pu

There have been many photofission measurements performed in the study of the fission process for the "big three" actinides. Most of the photofission cross-section data obtained with quasimonoenergetic γ-ray beams were measured at Lawrence Livermore National Laboratory (LLNL) in the USA and the Centre d'Etudes Nucléaires de Saclay (CEA Saclay) in France [8,14–16]. The photon beams produced at these facilities were from in-flight annihilation of relativistic positrons. Detailed studies of the photon-induced fission cross section on actinides have been carried out at LLNL by groups from LLNL and Los Alamos National Laboratory (LANL) [15,16]. In 1964, Bowman *et al.* [17] measured the photodisintegration cross sections of ^{235}U using photons obtained from the annihilation in flight of fast positrons at LLNL. Later, in 1980, Caldwell *et al.* [15] measured the photofission cross section for ^{235}U and ^{238}U (along with some other actinides) in the GDR region. Berman *et al.* [16] continued using the LLNL facility to measure the photofission cross section of other actinides, including ^{239}Pu. Photofission cross-section measurements on ^{238}U, ^{232}Th, and ^{237}Np at $E_\gamma = 8.0$–19.0 MeV were performed at the in-flight positron annihilation facility at CEA Saclay by Veyssière *et al.* [14] in 1973. These measurements were a part of a systematic investigation of photonuclear reactions in the GDR region at CEA Saclay. Using quasimonoenergetic photons from e^+ annihilation and direct fission fragment detection at the Giessen positron annihilation facility, Ries *et al.* [18] measured the absolute photofission cross section for ^{235}U and ^{238}U in the energy range from 11.5–30.0 MeV.

Photonuclear reaction data obtained using photons produced at in-flight positron annihilation facilities described above were complemented by measurements at lower energies using quasimonoenergetic γ rays produced by neutron-capture sources. With these sources, the photon beam axis and energy were selected by Compton scattering of the γ rays emitted from the capture reaction to a specific angle. For example, in 1973 Anderl *et al.* [19] reported photofission cross-section measurements on ^{235}U and ^{238}U at relatively low energy, $E_\gamma = 5.0$–8.0 MeV. The photons were obtained by Compton scattering of γ rays produced by neutron capture on nickel. Similarly, Moraes *et al.* [20] used thermal neutron capture γ rays in several targets placed at the core of a reactor to measure the photofission cross section of ^{239}Pu near the threshold region.

TABLE I. Previous measurements of the ^{235,238}U(γ, f) and ^{239}Pu(γ, f) reaction cross section at the GDR energy region.

First author	Year	E_γ range (MeV)	Beam
^{235}U			
Bowman [17]	1964	6.1–18.6	$e^+ + e^-$
Khan [23]	1972	5–8.4	(n,γ)
Anderl [19]	1973	5–8	(n,γ)
Caldwell [15]	1980	5.3–18.3	$e^+ + e^-$
Ries [18]	1984	11.5–30	$e^+ + e^-$
Soldatov [22]	1992	5.0–11	bremsstrahlung
^{238}U			
Katz [24]	1958	6.0–17.7	bremsstrahlung
Manfredini [25]	1966	5.4–8.9	(n,γ)
Bergere [26]	1972	7.8–18.3	bremsstrahlung
Veyssière [14]	1973	7.8–18.4	$e^+ + e^-$
Dickey [27]	1975	5.0–8.0	tagged-γ
Neto [28]	1976	6.3–52.0	bremsstrahlung
Koretskaya [29]	1979	8.0–20.0	bremsstrahlung
Caldwell [15]	1980	5.3–18.3	$e^+ + e^-$
Ries [18]	1984	11.5–30	$e^+ + e^-$
Soldatov [22]	1992	5.0–11	bremsstrahlung
^{239}Pu			
Katz [24]	1958	5.4–19.8	bremsstrahlung
Shapiro [21]	1971	7.5–11.0	bremsstrahlung
Berman [16]	1986	6.0–17.6	$e^+ + e^-$
Soldatov [22]	1992	5.0–10.9	bremsstrahlung
Moraes [20]	1993	5.4–9.7	(n,γ)

A substantial amount of the existing photofission data were obtained using a bremsstrahlung broad-energy beam. As shown in Table I, most of the data reported since 1990 were for measurements conducted with a bremsstrahlung beam. For example, Shapiro *et al.* [21] report data for photofission measurements on ^{239}Pu that were performed using bremsstrahlung beams. In addition, Soldatov *et al.* [22] measured the photofission cross section of ^{235}U and ^{238}U using bremsstrahlung. They also obtained relative photofission cross-section data for ^{238} and ^{239}Pu in the energy regime of 5–11 MeV.

The use of bremsstrahlung or even annihilation of in-flight fast positrons imposes some limitations and difficulties for the measurement and interpretation of photonuclear cross-section data. For example, using bremsstrahlung broad-energy beams, one has to increase the bremsstrahlung end-point energy in small increments to determine the excitation function [22]. This requires great stability in the accelerator parameters, enormous counting statistics, and high-precision knowledge of the flux of the bremsstrahlung energy spectrum, especially near the end-point energy. The latter one is hard to measure or to calculate reliably. In case of in-flight annihilation of fast positrons, the effects of the positron bremsstrahlung contaminant must be subtracted [16].

The main objective of these photofission studies has been to obtain nuclear fission information at excitation energies near the fission threshold and in the GDR region. The data are plagued by clear disagreements in both shape (i.e., energy

dependency) and magnitude of the cross section. Furthermore, these disagreements exist not only between data obtained using different methods, but also for data obtained using the same method. These differences were larger than the reported statistical uncertainties. Most of these photonuclear reaction cross-section data are included in the evaluated databases [30,31], resulting in large systematic uncertainties. New data sets obtained using techniques based on modern technologies are needed to improve the accuracy and reliability of the cross-section data used in the evaluated databases.

As pointed out by several authors [18], reliable data on photofission cross sections can only be obtained using monoenergetic photon sources with good resolution and sufficient intensity. In the present work, we report on our high-accuracy measurements of the cross-section ratios for photofission of ^{235,238}U and ^{239}Pu. The measurements were carried out using monoenergetic photon beams provided by the High Intensity γ-ray Source (HIγS) facility at the Triangle Universities Nuclear Laboratory (TUNL). The techniques employed in this work eliminate the difficulties associated with using bremsstrahlung beams and beams produced by positron in-flight annihilation. The technical details of this work have been discussed in Ref. [32]. The sections to follow describe and discuss the main features of the experimental methods, the data analysis and results, and the comparison of our photofission results with data from neutron-induced fission measurements, and conclude with a summary of our results and findings.

III. EXPERIMENTAL TECHNIQUE AND DUAL-FISSION CHAMBER

Details on the HIγS facility can be found in Ref. [33] and are briefly summarized here. The HIγS facility produces a quasimonoenergetic Compton backscattered photon beam with a wide and tunable energy range and either linear or circular polarization. A high-flux photon beam is created by colliding relativistic electron beam bunches circulating in a storage ring with photon pulses inside the high-power optical cavity of a free-electron laser (FEL). For this experiment 450 and 540 nm FEL wavelength photons and 400–650 MeV electrons were used to provide high-energy photon beams between 9.0 and 17.0 MeV. The peak energy of the photon beam was selected by an Al collimator of length 44.5 cm with a cylindrical hole of 1.905 cm diameter and positioned 55 meters downstream from the FEL photon-electron collision point in the storage ring. This collimator diameter results in an energy spread of ∼2.5% (FWHM) of the photon beam.

Aluminum was chosen as the collimator material to minimize the number of neutrons produced via the (γ,n) reaction because of its high neutron separation energy of 13.6 MeV. Figure 1 shows a schematic diagram of the experimental setup in the upstream target room experimental area of the HIγS facility. The principal task in obtaining accurate fission cross-section data is the precise quantitative determination of the number of fissions, which occur during the measurements. This was accomplished using a specially fabricated dual-fission ionization chamber (DFC) [34], as seen in the layout of the experimental setup (Fig. 1). In its normal configuration, the DFC contains a thick activation target at its center, sandwiched

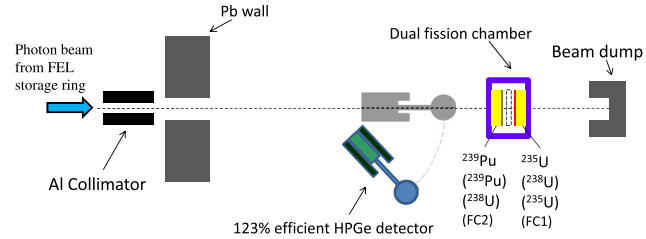

FIG. 1. Schematic diagram (not to scale) of the experimental setup using a dual-fission chamber and a 123% efficient (relative) HPGe detector. In the present photofission measurement, the thick activation target was not used (shown by the dashed-line at the center of the fission chamber).

by two thin reference foils of the same isotope in the front and back chambers of the DFC. These chambers have been extensively used at TUNL to perform systematic investigations of fission product-yield measurements with monoenergetic neutron beams [34,35]. In the present measurements, the thick activation target was not in place [32]. Two reference foils of ^{235}U, ^{238}U, and ^{239}Pu were used in the downstream (FC1) and upstream (FC2) fission chamber (FCs), respectively (see Table II). By taking the ratio of the number of fissions in each chamber, the necessity of knowing the photon flux is eliminated, as the same collimated photon beam passes through both FCs. In addition, the nearly ideal parallel photon beam incident on the target position eliminates the need for a source-target angular-correlation correction. This is due to the long distance (∼60 m) between the FEL collision point and the DFC. Details of a DFC can be found in Refs. [32,34,35]. The signals from each of the FCs are sent to a manifold via a UT-085 semirigid coaxial cable and from there to Ortec 142-PC preamplifiers. The preamplified signals are then sent to a Canberra 2026 spectroscopic amplifier and then fed to a Canberra Multiport II multichannel analyzer, supported by the GENIE2000 software [36].

The reference foils are electroplated on 0.013 cm thick Ti disks. The active area of the deposit is 1.27 cm in diameter, which is about 7.0 mm smaller than the photon beam diameter at the target, thereby allowing an alignment tolerance of ±3.5 mm, which is well within our capabilities. In addition, photon beam imaging was performed at the DFC position

TABLE II. Information on the actinide reference foils used in the individual FCs. Diameter of each reference foil is 1.27 cm.

Foil	Chamber	Mass (μg)	Isotopic abundance (%)
^{235}U/^{238}U setup			
^{235}U	FC1	160.36(160)	99.835(2)
^{238}U	FC2	121.90(122)	99.998(2)
^{235}U/^{239}Pu setup			
^{235}U	FC1	160.36(160)	99.835(2)
^{239}Pu	FC2	8.52(3)	99.954(2)
^{238}U/^{239}Pu setup			
^{238}U	FC1	121.90(122)	99.998(2)
^{239}Pu	FC2	8.52(3)	99.954(2)

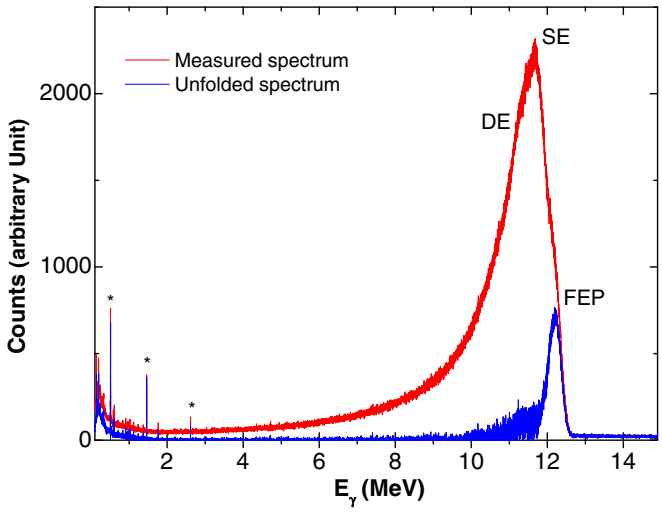

FIG. 2. γ-ray spectrum (in red) measured with a 123% HPGe detector positioned at 0° relative to the incident photon beam of 12.25 MeV. The full-energy peak (FEP), single escape (SE), and double escape (DE) are labeled. In the low-energy part of the spectrum, room background lines (indicated by the asterisk) are clearly seen. Taking the HPGe detector response into account, the unfolded spectrum of the FEP (shown in blue) is obtained.

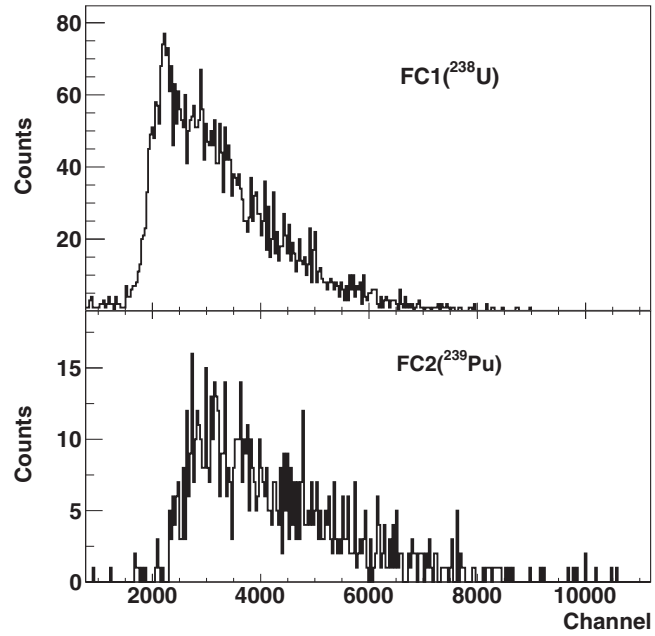

FIG. 3. Fission chamber pulse-height spectra for the downstream (FC1) and upstream (FC2) chambers are shown for 11.2 MeV incident photon beam. These chambers were loaded with ^{238}U and ^{239}Pu reference foils, respectively.

using an imaging system [37,38]. This imaging system has sub-mm spatial resolution (better than 0.5 mm) and a high contrast sensitivity (better than 5%). Table II gives detailed information about the reference foils used in the present work. The masses of the reference foils were determined at LANL by α spectroscopy using well-calibrated ionization chambers.

The incident photon flux varied between approximately $2 \times 10^7 \gamma/(\text{cm}^2\text{s})$ at 9 MeV and $8 \times 10^7\ \gamma/(\text{cm}^2\text{s})$ at 15 MeV, before dropping to $5 \times 10^7\ \gamma/(\text{cm}^2\text{s})$ at the highest energy used in the present experiment. The photon flux was obtained from a calibrated plastic scintillator paddle. The paddle itself was calibrated with respect to a 8 in diameter×12 in long NaI detector of known efficiency.

IV. DATA ANALYSIS AND RESULTS

For the present measurements circularly polarized photon beams of energies ranging from 9.0 to 17.0 MeV were used. The energy distribution of the incident photon beam was measured with a large volume high-purity germanium (HPGe) detector of efficiency 123% (relative to a standard 7.62cmx7.62cm NaI detector) that was positioned on the beam axis upstream of the fission chamber. During beam-energy measurements, the beam intensity was reduced by a series of copper attenuators mounted upstream, approximately 45 m from the location of the DFC. The variation in the attenuation coefficient is negligible over the narrow energy width of the beam, resulting in the negligible distortion in the beam energy profile. A typical energy distribution of the incident beam is shown in Fig. 2. The measured energy spectrum was deconvoluted using the detector response function to determine the beam energy profile. An example of the unfolded energy spectrum is shown in Fig. 2.

The FWHM resolution of the beam at 12.25 MeV is ~240 keV (~2.0%). The uncertainty in beam centroid energy is less than ±10 keV. After the beam-energy measurement, the HPGe detector and attenuators were moved to an off-axis position during the actual cross-section ratio measurements.

Typical pulse-height fission spectra produced by the DFC during photon irradiation are shown in Fig. 3. Each spectrum was integrated to give the total number of fissions measured in the individual chamber for a given photon energy. From these numbers, the fission cross-section ratio was computed using the formula:

$$\left(\frac{\text{Act1}}{\text{Act2}}\right)_{CS} = \frac{(N)_{\text{Act1}} \times (M)_{\text{Act1}}}{(N)_{\text{Act2}} \times (M)_{\text{Act2}}} \times \frac{(m)_{\text{Act2}} \times (t)_{\text{Act2}}}{(m)_{\text{Act1}} \times (t)_{\text{Act1}}}, \quad (1)$$

where Act stands for one of the actinide samples, N is the number of fission counts, M is the molar mass, m is the areal mass density of the foil, and t is the live time of the data-acquisition system. It should be noted that the attenuation of the photon beam from FC2 to FC1 is practically zero at these incident energies. As can be derived from Eq. (1), the main statistical error in the (Act1/Act2) cross-section ratio is due to the relative uncertainties in the number of counts collected from each chamber and represents the largest source of uncertainty for all sets of measurements. The systematic error is due to the uncertainty in the ratio of the mass densities of the DFC foils and is estimated to be up to 2%.

Our measured ^{235}U/^{238}U, ^{235}U/^{239}Pu, and ^{238}U/^{239}Pu fission cross-section ratios are tabulated in Tables III, IV, V and plotted in Figs. 4, 5, and 6 (as upsidedown triangles). The error bars on our data points in the figures and the tables represent

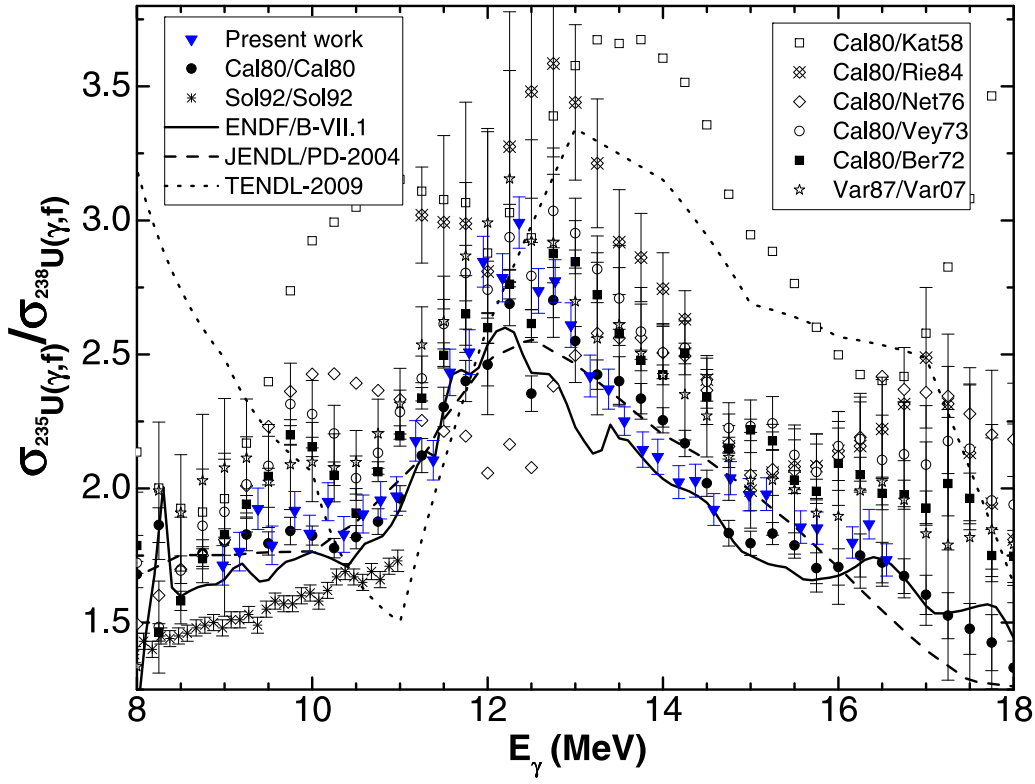

FIG. 4. Experimental fission cross-section ratios for $^{235}U/^{238}U$ are compared with previous measurements [14,15,18,22,24,26,28,39] and the ENDF/B-VII.1 [30] and JENDL/PD-2004 [31] evaluations, and the TENDL-2009 [30,31] calculation. The error bars on our data points represent the total experimental uncertainties.

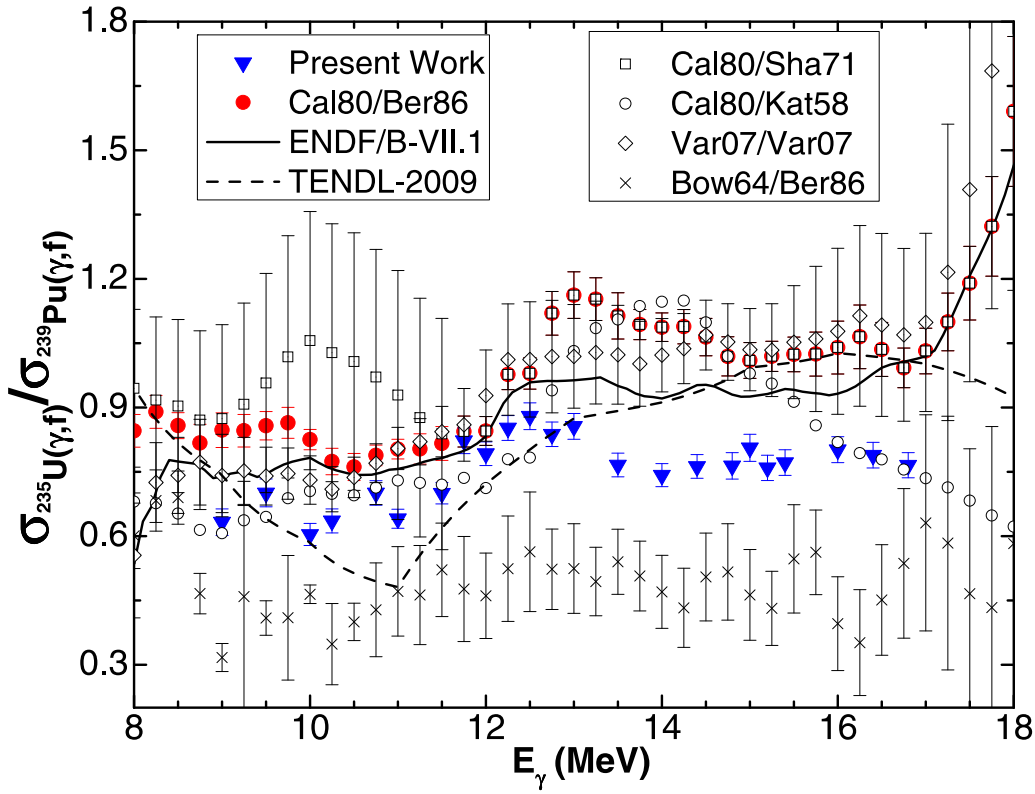

FIG. 5. Experimental fission cross-section ratios for $^{235}U/^{239}Pu$ are compared with previous measurements [15,16,18,22,24,26,28,39] and the ENDF/B-VII.1 [30] evaluation, and the TENDL-2009 [30,31] calculation. The error bars on our data points represent the total experimental uncertainties.

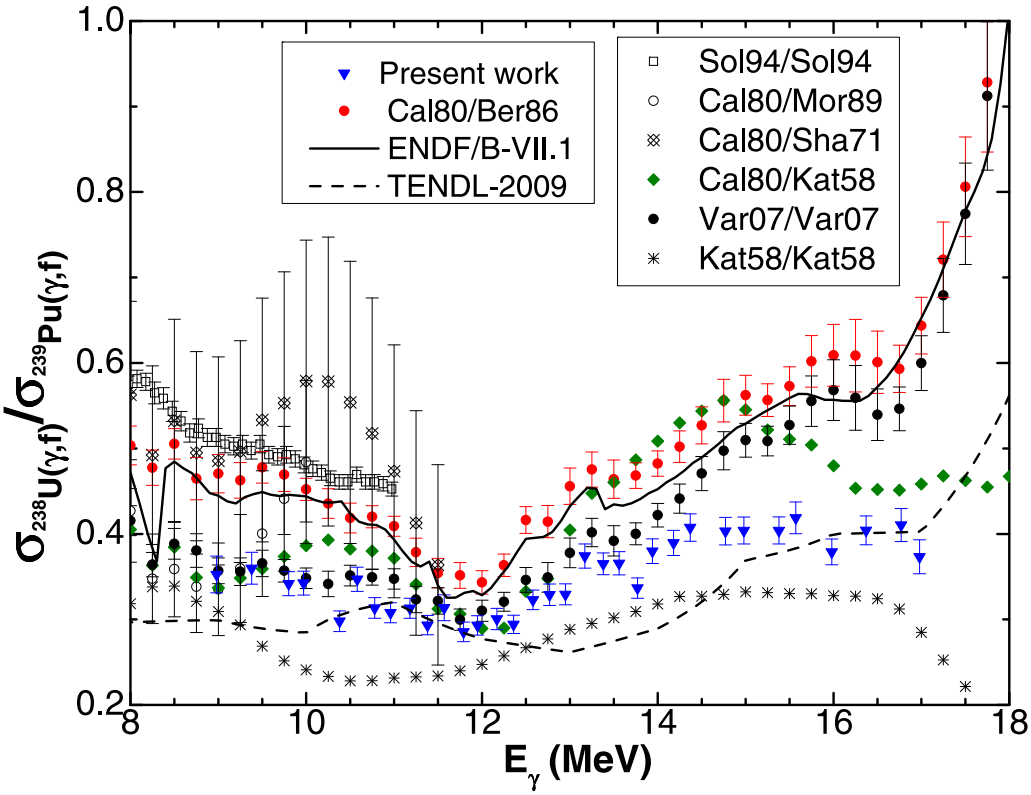

FIG. 6. Experimental fission cross-section ratios for ^{238}U/^{239}Pu are compared with previous measurements [14,15,18,22,24,26,28,39] and the ENDF/B-VII.1 [30] evaluation and the TENDL-2009 [30,31] calculation. The error bars on our data points represent the total experimental uncertainties.

the total experimental uncertainties, which were computed by adding statistical and systematic uncertainties in quadrature. The energy spread in the measurement at each γ-ray beam energy was between 200 and 400 keV FWHM, which is not shown in the plots for consistency with the literature data to which we compare our data. Also shown in these figures are the ratios computed from the ^{235}U cross-section data of Bowman *et al.* [17], Caldwell *et al.* [15], Ries *et al.* [18], and Soldatov *et al.* [22]; the ^{238}U cross-section data of Katz *et al.* [24], Bergere *et al.* [26], Veyssière *et al.* [14], Neto *et al.* [28], Caldwell *et al.* [15], Ries *et al.* [18], and Soldatov *et al.* [22]; and the ^{239}Pu cross-section data of Katz *et al.* [24], Shapiro *et al.* [21], Berman *et al.* [16], Moraes *et al.* [20], and Soldatov *et al.* [22]. These previous data for ^{235}U, ^{238}U, and ^{239}Pu were interpolated or extrapolated to correspond to the incident photon energies used in the present work. The predictions based on the evaluations ENDF/B-VII.1, JENDL/PD-2004, and TENDL-2009 [30] are also shown in the plots. Varlamov *et al.* [39] compiled the previously available experimental data on the photofission cross sections and published the evaluated values for all three actinides. These evaluated values are also shown in the plots.

We now compare our data with those of the recent measurements and data evaluations. In Figs. 7, 8, and 9 the number of data sets from the previous measurements are limited to those that are most consistent with the latest evaluations. In addition to focusing on the most relevant data this selection of the data sets reduces the clutter in the plots and enables easier

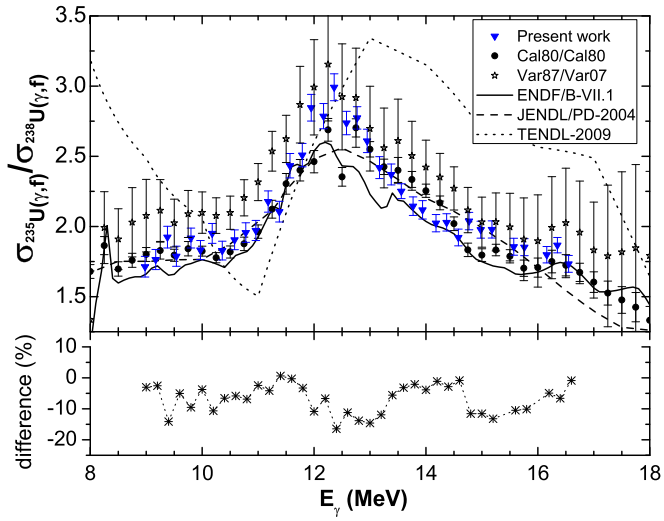

FIG. 7. Experimental fission cross-section ratios for ^{235}U/^{238}U are compared with the previous measurements [15,39] and the evaluations ENDF/B-VII.1 [30], JENDL/PD-2004 [31], and the TENDL-2009 [30,31] calculation. The error bars on our data points represent the total experimental uncertainties. Also shown (in the bottom panel) are the differences (in %) between the ENDF/B-VII.1 evaluation and our present data. The relative difference in our data and the ENDF/B-VII.1 evaluation range from 0% to about 16% (the average deviation is ~6.8%) with our data constantly higher than the evaluation values.

TABLE III. Photofission cross-section ratio data for $^{235}U/^{238}U$ obtained in the present experiment. The uncertainties are the total experimental uncertainties associated with the present measurements.

E_γ (MeV)	$\sigma(^{235}U(\gamma,f)/^{238}U(\gamma,f))$	uncertainty
8.98	1.713	0.074
9.17	1.765	0.072
9.38	1.924	0.077
9.54	1.788	0.072
9.77	1.918	0.071
9.97	1.832	0.068
10.18	1.951	0.071
10.36	1.829	0.067
10.58	1.905	0.070
10.78	1.956	0.070
10.96	1.972	0.072
11.18	2.178	0.075
11.38	2.105	0.074
11.57	2.433	0.087
11.79	2.508	0.084
11.95	2.846	0.095
12.17	2.786	0.090
12.36	2.992	0.096
12.58	2.737	0.083
12.77	2.774	0.079
12.95	2.610	0.083
13.17	2.420	0.078
13.38	2.370	0.075
13.56	2.251	0.053
13.77	2.145	0.066
13.94	2.118	0.066
14.18	2.024	0.061
14.37	2.029	0.061
14.58	1.922	0.059
14.77	2.039	0.062
14.98	1.977	0.060
15.18	1.979	0.061
15.57	1.856	0.060
15.76	1.852	0.060
16.16	1.799	0.059
16.35	1.867	0.055
16.55	1.734	0.060

interpretation. Comparisons for each data set are discussed below. Our measurements of the $^{238}U/^{239}Pu$ cross-section ratios allowed an assessment of the systematic error in the experimental technique to the precision of the statistical accuracy. This measurement is redundant because this ratio can be computed from our measurements of the $^{235}U/^{238}U$ and $^{235}U/^{239}Pu$ cross-section ratios. Standard average deviation in the difference between the measured and the computed ratios is ∼2%, which is consistent with the systematic uncertainty in the present measurement.

A. $^{235}U/^{238}U$ cross-section ratio

Figure 4 presents the existing information for the $^{235}U/^{238}U$ cross-section ratio. It should be pointed out that in contrast to our work, all previous determinations of the $^{235}U/^{238}U$

TABLE IV. Photofission cross-section ratio data for $^{235}U/^{239}Pu$ obtained in the present experiment. The uncertainties are the total experimental uncertainties associated with the present measurements.

E_γ (MeV)	$\sigma(^{235}U(\gamma,f)/^{238}U(\gamma,f))$	uncertainty
8.98	0.621	0.031
9.48	0.707	0.033
9.97	0.584	0.026
10.23	0.636	0.028
10.72	0.710	0.029
10.96	0.624	0.022
11.48	0.700	0.025
11.73	0.822	0.030
11.95	0.792	0.028
12.23	0.852	0.029
12.47	0.880	0.031
12.73	0.838	0.028
12.95	0.856	0.030
13.48	0.766	0.028
14.96	0.742	0.027
14.37	0.763	0.028
14.77	0.764	0.031
14.98	0.826	0.032
15.18	0.759	0.029
15.57	0.772	0.030
15.98	0.802	0.030
16.37	0.789	0.030
16.77	0.765	0.029

cross-section ratios are derived from independent cross-section measurements of ^{235}U and ^{238}U and not from a simultaneous measurement of both cross sections as in our case. The present

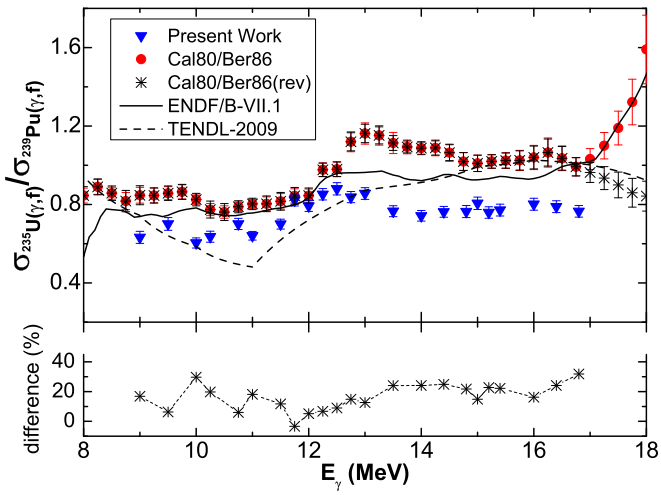

FIG. 8. Experimental fission cross-section ratios for $^{235}U/^{239}Pu$ are compared with the previous measurements [15,16] and the evaluation ENDF/B-VII.1 [30] and the TENDL-2009 [30,31] calculation. The error bars on our data points represent the total experimental uncertainties. Also shown (in the bottom panel) are the differences (in %) between the ENDF/B-VII.1 evaluation and our present data. The relative difference in our data and the ENDF/B-VII.1 evaluation range up to 32% (the average deviation is ∼16%) with our data constantly lower than the evaluation values.

TABLE V. Photofission cross-section ratio data for $^{238}U/^{239}Pu$ obtained in the present experiment. The uncertainties are the total experimental uncertainties associated with the present measurements.

E_γ (MeV)	$\sigma(^{235}U(\gamma,f)/^{238}U(\gamma,f))$	uncertainty
8.98	0.353	0.021
9.38	0.360	0.019
9.77	0.342	0.014
9.97	0.343	0.014
10.38	0.298	0.012
10.58	0.347	0.014
10.78	0.313	0.012
10.96	0.308	0.012
11.18	0.313	0.012
11.38	0.293	0.011
11.57	0.314	0.015
11.79	0.285	0.011
11.95	0.293	0.011
12.17	0.301	0.012
12.36	0.294	0.011
12.58	0.323	0.011
12.77	0.329	0.013
12.95	0.329	0.012
13.17	0.374	0.014
13.38	0.365	0.013
13.56	0.366	0.014
13.77	0.337	0.012
13.94	0.380	0.014
14.18	0.390	0.015
14.37	0.408	0.016
14.77	0.403	0.016
14.98	0.404	0.016
15.38	0.404	0.016
15.57	0.419	0.019
15.98	0.379	0.015
16.37	0.404	0.017
16.77	0.410	0.019
16.98	0.373	0.020

measured cross-section ratios reach a maximum value of 2.992(96) at $E_\gamma = 12.4$ MeV. Above this energy, the cross-section ratio drops smoothly with a small bump at $E_\gamma \sim 15$ MeV. A similar trend is seen in the previous measurements of Caldwell *et al.* [15], labeled Cal80/Cal80, except for the data at $E_\gamma \sim 12.5$ MeV. The ratios involving the ^{235}U and ^{238}U data of Soldatov and Smirenkin [22], labeled Sol92/Sol92, have very small uncertainties, and are lower in magnitude than any of the other data in the 8–11 MeV photon energy range. The compilation work of Varlamov *et al.* [39], labeled Var87/Var07, had fairly large uncertainties and provides ratios, which are larger throughout the entire energy range, especially below 10 MeV, but the general trend is in good agreement with the present work. All other ratios shown in Fig. 4 are based on the ^{235}U data of Caldwell *et al.* [15]. Using the early ^{238}U data of Katz *et al.* [24], large ratios (labeled Cal80/Kat58 and plotted without uncertainties) are obtained. The ^{238}U data of Ries *et al.* [18] (labeled Cal80/Rie84) also provide fairly large ratios, but follow the general trend of our data and the Cal80/Cal80 ratios,

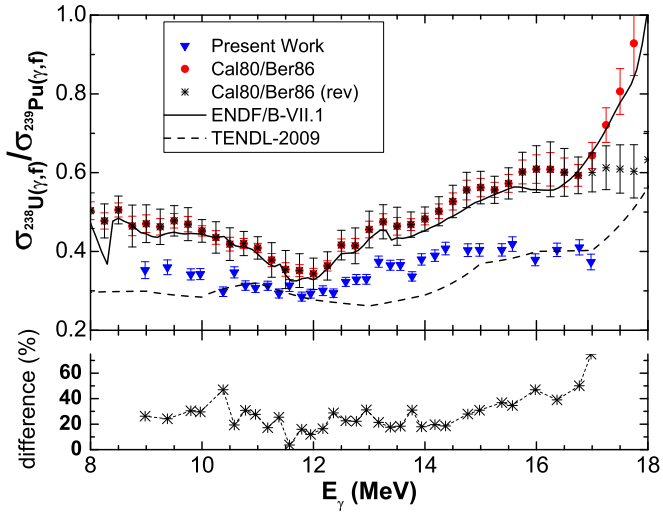

FIG. 9. Experimental fission cross-section ratios for $^{238}U/^{239}Pu$ are compared with previous measurements [15,16] and the evaluation ENDF/B-VII.1 [30] and the TENDL-2009 [30,31] calculation. The error bars on our data points represent the total experimental uncertainties. Also shown (in the bottom panel) are the differences (in %) between the ENDF/B-VII.1 evaluation and our present data. The relative difference in our data and the ENDF/B-VII.1 evaluation range from 0 to 70% (the average deviation is ~25%) with our data constantly much lower than the evaluation values, except for the energy regime around 12 MeV.

except for energies above 16 MeV. The ratios involving the ^{238}U data of Neto *et al.* [28] (labeled Cal80/Net76) between 9 and 12.5 MeV give too large values below 11 MeV and too low values above 11.5 MeV, again in comparison to the present ratios and those of Cal80/Cal80. The ratios based on the ^{238}U data of Veyssière *et al.* [14] (labeled Cal80/Vey73) are larger throughout the entire energy range, especially below 10 MeV and above 16 MeV. Finally, the ratios using the ^{238}U data of Bergere *et al.* [26] (labeled Cal80/Ber72) follow the general trend and magnitude provided by our data and those of Cal80/Cal80 very well, except in the 9 MeV energy range and above 16 MeV.

The ENDF/B-VII.1 evaluation [30], although on the average lower than our data, is in reasonably good agreement with the present measurements, except for the region close to $E_\gamma \sim 12.0$–13.5 MeV, where the measured ratios are considerably higher than the evaluation. The JENDL/PD-2004 [31] calculation is smoother and provides a fair representation of our data, except for the underestimation in the vicinity of 12 MeV. In contrast, the TENDL-2009 [30,31] model calculation gives a poor representation of the data and is ruled out. At energies around 12–13 MeV our data indicate that the photofission cross section for ^{235}U is larger relative to that for ^{238}U than is given by the ENDF/B-VII.1 evaluation [30].

B. $^{235}U/^{239}Pu$ cross-section ratio

The cross-section ratio data obtained in the present work for $^{235}U/^{239}Pu$ at 23 photon energies between 9–17 MeV are shown in Fig. 5 (upsidedown triangles) in comparison

to the previous literature data. The results are tabulated in Table IV. Our cross-section ratio values are more or less constant over the entire energy range, except for a small bump at $E_\gamma \sim 12.5$ MeV. The ratios of Varlamov *et al.* [39] (labeled Var07/Var07) compilation work are close to our data up to approximately 13 MeV, but beyond this energy remain at about 1.05, before increasing considerably above 16 MeV. In addition, the uncertainty of the data is very large above 16 MeV. The ratio based on the ^{235}U data of Bowman *et al.* [17] and the ^{239}Pu data of Berman *et al.* [16] labeled Bow64/Ber86 are very low and structureless throughout the entire energy range. The uncertainties are comparable to those of Var07/Var07. The ^{235}U data of Caldwell *et al.* [15] combined with the very early ^{239}Pu data of Katz *et al.* [24] and labeled Cal80/Kat58 provide ratios that are in good agreement with our data up to 12.5 MeV, but then continue to increase before turning around, meeting our data again in the 16 MeV energy regime. The uncertainties are not assigned to the Cal80/Kat58 ratios. The ^{235}U data of Caldwell *et al.* [15] and the ^{239}Pu data of Shapiro *et al.* [21], labeled Cal80/Sha71, are restricted to energies below 11.5 MeV. They have very large uncertainties and seem to peak at 10 MeV, a trend not seen in any of the other ratios shown in Fig. 5. Finally, the ^{235}U data of Caldwell *et al.* [15] combined with the ^{239}Pu data of Berman *et al.* [16] labeled Cal80/Ber86, give ratios that are comparable with our present data. These Cal80/Ber86 ratios are large in magnitude throughout the entire energy range, especially above 13 MeV and with an additional sharp increase above 17 MeV.

It is important to note that the last data point (at $E_\gamma = 17.76$ MeV) of the ^{239}Pu cross section measured by Berman *et al.* [16] has a considerably lower value than the previous one at $E_\gamma = 16.78$ MeV. This drop in cross section resulted in the sharp rise in the ^{235}U/^{239}Pu cross-section ratio (see Fig. 8).

Also shown in Fig. 8 are the revised cross-section ratio values (Cal80/Ber86-rev) for ^{235}U/^{239}Pu, in which the last data point of the ^{239}Pu cross section was ignored. As can be seen, the positive slope of the ^{235}U/^{239}Pu cross-section ratio turned into a negative slope. Unfortunately, we do not have data for energies beyond 17 MeV.

The ENDF/B-VII.1 evaluation [30] is in good agreement with the Var07/Var07 and also close to Cal80/Ber86, but is well above our data below 11 MeV and especially above 13 MeV. The TENDL-2009 [30,31] model calculation provides ratios that are in fair agreement with our data below 13.5 MeV, but overshoots our data above this energy.

As is seen in Fig. 8, the ENDF/B-VII.1 evaluation [30] is in general about 0–32 % larger than our measured ratios over the whole energy range of our experiment with the average deviation of about 16%. This suggests that the ^{235}U cross section is about 16% smaller than that for ^{239}Pu over 9–17 MeV energy range.

C. ^{238}U/^{239}Pu cross-section ratio

The ^{238}U/^{239}Pu fission cross-section ratios were measured at 33 photon energies between 9 to 17 MeV and are tabulated in Table V and plotted in Figs. 6 and 9. The early ^{238}U/^{239}Pu ratios of Katz *et al.* [24], labeled Kat58/Kat58, are low in magnitude throughout the entire present experimental energy range. They are shown in Fig. 6 without error bars. The ratios based on the compilation work of Varlamov *et al.* [39] (labeled Var07/Var07) are in very close agreement with our data up to 14 MeV. Beyond this energy the ratios increase dramatically, while the ratios measured in the present work remain constant. The uncertainties associated with both ratios are comparable. The ratios obtained from the data of Soldatov and Smirenkin [22], labeled Sol92/Sol92, are restricted to energies below 11 MeV. They have very small uncertainties but are much higher in magnitude than our data. The remaining ratios shown in Fig. 6 all involve the ^{238}U data of Caldwell *et al.* [15]. Combining these with the ^{239}Pu data of Katz *et al.* [24], provide the ratios labeled Cal80/Kat58, are given without error bars in Fig. 6. These ratios are close to our data up to approximately 13 MeV. Beyond this energy the ratios keep increasing before turning around at 15 MeV. Our data do not show such an energy dependency. The ratio calculated from the ^{238}U data of Caldwell *et al.* [15] and the ^{239}Pu data of Shapiro *et al.* [21] are restricted to energy below 11.5 MeV. They have large uncertainties, and are larger in magnitude than all other data in this energy range. Using instead the ^{239}Pu data of Moraes *et al.* [20] gives the ratios labeled Cal80/Mor89 shown in Fig. 6. below 10 MeV, is close agreement with the ratios Cal80/Kat58, Var07/Var07, our ratios, and at the lowest energies also with Kat58/Kat58. Finally, combining the ^{238}U data of Caldwell *et al.* [15] with those of Berman *et al.* [16] provides the ratios labeled Cal80/Ber86. They are well above our ratios (Fig. 9), but below the trend of Cal80/Kat58 between approximately 10 MeV and 15.5 MeV, and Var07/Var07 between 10.5 and 17.5 MeV, with very good agreement above 15 MeV.

As has been discussed already in Sec. IV B, a possibly questionable datum of Berman *et al.* [16] is responsible for the steep increase in the ratio seen in Fig. 9 at the highest energies. Ignoring this datum results in smaller ratios, labeled Cal80/Ber86(rev) in Fig. 9.

The ENDF/B-VII.1 evaluation basically follows Cal80/Ber86, and splitting the difference between Var07/Var07 and Cal80/Ber86 between 14 and 16 MeV. The ENDF/B-VII.1 evaluation ratios are higher than our data across the entire energy range of our experiment. The shapes of the Cal80/Ber86 data and the ENDF/B-VII.1 evaluation have a more pronounced dip at around 12 MeV than our data. The TENDL-2009 model calculation provides low ratios, but on the average is close to our data than ENDF/B-VII.1.

Our present data suggest that the photofission cross section for ^{238}U is smaller than that for ^{239}Pu by about 25% compared to the prediction of the ENDF/B-VII.1 evaluation over the energy range of our experiment.

V. COMPARISON TO NEUTRON-INDUCED FISSION

The present work is part of a study to investigate the effects of the incoming probe (e.g., neutron versus photon) on nuclear fission observables [32,40,41]. The measured cross-section ratios for the three actinides are compared for nuclear fission induced with photons and neutrons [42–44] (see Fig. 10).

For the ^{238}U/^{239}Pu cross section ratio [see Fig. 10(a)] our (γ, f) ratios are considerably lower than the (n, f) ratios of Tovesson *et al.* [42,43]. This observation requires further study, because not only the compound nuclei are different but

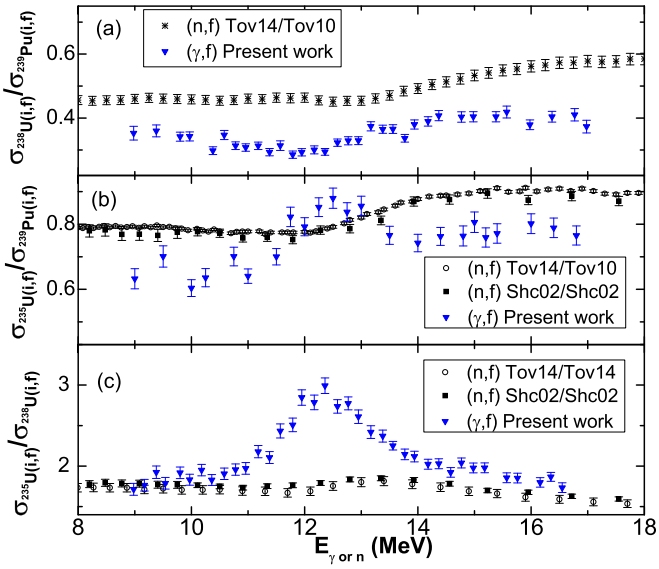

FIG. 10. Present photon-induced cross-section ratio data are compared to their neutron-induced counterparts [42–44].

also the excitation energies. The same arguments hold for the ^{235}U/^{239}Pu [see Fig. 10(b)] and ^{235}U/^{238}U [see Fig. 10(c)] ratios, where distinct differences are seen, especially for the ^{235}U/^{238}U ratios using data from Tovesson *et al.* [42,43] and Shcherbakov *et al.* [44]. However, a detailed study of these very interesting observations are beyond the scope of the present work.

VI. SUMMARY AND CONCLUSION

In this paper we report high-accuracy and self-consistent photofission cross-section ratio measurements carried out on the ^{235}U, ^{238}U, and ^{239}Pu isotopes in the energy range from 9.0 to 17.0 MeV. Data were measured at each energy to statistical and systematical accuracies better than ±5 % and ± 2%, respectively. This is substantial improvement over previous measurements.

Monoenergetic photon beams were provided by the HIγS facility at TUNL. A dual-fission ionization chamber was employed to measure the total fission events from thin reference foils of these actinides. Using this approach most systematic uncertainties cancel, in contrast to ratios computed from previously published cross-section data.

Our cross-section ratio data are compared with the ratios computed from the published individual cross-section data and were found to be more or less in good agreement with the Caldwell *et al.* [15] data for ^{235}U/^{238}U (see Fig. 7). The ENDF/B-VII.1 evaluation for ^{235}U/^{238}U, although on the average lower than our data, is in reasonably good agreement with the energy trend of the present measurements, except in the E_γ ∼ 12.0–13.5 MeV energy region. The JENDL/PD-2004 evaluation provided a fair description of our data, while the TENDL-2009 model description is unsatisfactorily.

Our ^{235}U/^{239}Pu cross-section ratios are considerably different from all of the existing sets of ratios, especially between 13 and 16.5 MeV. This observation includes the ratios calculated from the ^{235}U data of Caldwell *et al.* [15] and the ^{239}Pu data of Berman *et al.* [16] (labeled Cal80/Ber86), questioning the quality of the ^{239}Pu data. Surprisingly, the ENDF/B-VII.1 evaluation (Fig. 8) almost splits the difference between our data set and the Cal80/Ber86 ratios, while the TENDL-2009 model calculation is very different near 11 MeV.

The present ^{238}U/^{239}Pu cross-section ratios are in considerably better agreement with the ratios of Varlamov *et al.* [39] (labeled Var07/Var07) compilation work up to around 14.5 MeV than with those obtained from the ^{238}U data of Caldwell *et al.* [15] and ^{239}Pu data of Berman *et al.* [16] (labeled Cal80/Ber86), which are much lower in magnitude. Above this energy our ratios remain constant, while those of Var07/Var07 and Cal80/Ber86 are still increasing. The ENDF/B-VII.1 evaluation (Fig. 8) closely follows the ratios of Cal80/Ber86, while the TENDL-2009 model calculation provides ratios, which, on the average, are lower than our present data.

Summarizing our findings, we point out once more that the present photofission cross-section ratio data for the big three actinides were obtained in the same measurements using a dual-fission chamber loaded with the two actinide foils of interest. Using this unique approach many systematic uncertainties cancel out, especially the knowledge of the incident photon flux. Therefore, the actinide cross-section ratios obtained in the present work are expected to be considerably more accurate and self-consistent than any of the previous reported ratios, which are based on individual fission cross-section measurements.

In general our measurements of the relative photofission cross sections for ^{235}U and ^{238}U agree with the ENDF/B-VII.1 evaluation. However, we found that the photofission cross section for ^{239}Pu is larger than that for both ^{235}U and ^{238}U than is currently used in the ENDF/B-VII.1 evaluation.

ACKNOWLEDGMENTS

This work was supported partially by the US Department of Energy, Office of Nuclear Physics, under Grant No. DE-FG02-97ER41033, and by the National Nuclear Security Administration under the Stewardship Science Academic Alliance Program through the US Department of Energy, Grant No. DE-NA0002793, and performed under the auspices of the US Department of Energy by Lawrence Livermore National Laboratory under Contract No. DE-AC52-07NA27344.

[1] O. Hahn and F. Strassmann, Naturwissenschaften **27**, 11 (1939).

[2] L. Meitner and O. R. Frisch, Nature (London) **143**, 471 (1939).

[3] D. P. Wells, C. R. Segebade, and P. L. Cole, AIP Conf. Proc. **1265**, 379 (2010).

[4] J. Tickner, R. Bencardino, and G. Roach, Nucl. Instrum. Methods Phys. Res. Sec. B **268**, 99 (2010).

[5] H. Naik, S. V. Suryanarayana, K. C. Jagadeesan, S. V. Thakare, P. V. Joshi, V. T. Nimje, K. C. Mittal, A. Goswami, V. Venugopal, and S. Kailas, J. Radiol. Nucl. Chem. **295**, 807 (2013).

[6] M. Gmar, F. Jeanneau, H. Makil, B. Poumaréde, and F. Tola, Appl. Radiation Isotopes **63**, 613 (2005).

[7] P. M. Dighe, E. Berthoumieux, D. Doré, J. M. Laborie, X. Ledoux, V. Macary, S. Panebianco, and D. Ridikas, Annals Nucl. Energy **36**, 399 (2009).

[8] A. V. Varlamov, V. V. Varlamov, D. S. Rudenko, and M. E. Stepanov, INDC(NDS)-394, 1999, https://www-nds.iaea.org/publications/indc/indc-nds-0394.pdf.

[9] J. Silano, H. J. Karwowski, S. Clarke, S. Pozzi, S. Banerjee, D. Haden, G. Golovin, S. Chen, I. Ghebregziabher, C. Liu, C. Petersen, J. Zhang, N. Powers, B. Zhao, K. Brown, J. Mills, and D. Umstadter, in *IEEE International Conference on Technologies for Homeland Security (HST) 2013* (IEEE, Piscataway, NJ, 2013), p. 429.

[10] C. Liu, G. Golovin, S. Chen, J. Zhang, B. Zhao, D. Haden, S. Banerjee, J. Silano, H. Karwowski, and D. Umstadter, Opt. Lett. **39**, 4132 (2014).

[11] C. G. R. Geddes, S. Rykovanov, N. H. Matlis, S. Steinke, J.-L. Vay, E. H. Esarey, B. Ludewigt, K. Nakamura, B. J. Quiter, C. B. Schroeder, C. Toth, and W. P. Leemans, Nucl. Instrum. Methods Phys. Res. Sec. B **350**, 116 (2015).

[12] C. Wagemans, *The Nuclear Fission Process* (CRC Press, Boca Raton, 1991).

[13] E. Jacobs and U. Kneissl, in *The Nuclear Fission Process*, edited by C. Wagemans (CRC Press, Boca Raton, 1991), p. 103.

[14] A. Veyssière, H. Beil, R. Bergère, P. Carlos, A. Lepretre, and K. Kernbath, Nucl. Phys. A **199**, 45 (1973).

[15] J. T. Caldwell, E. J. Dowdy, B. L. Berman, R. A. Alvarez, and P. Meyer, Phys. Rev. C **21**, 1215 (1980).

[16] B. L. Berman, J. T. Caldwell, E. J. Dowdy, S. S. Dietrich, P. Meyer, and R. A. Alvarez, Phys. Rev. C **34**, 2201 (1986).

[17] C. D. Bowman, G. F. Auchampaugh, and S. C. Fultz, Phys. Rev. **133**, B676 (1964).

[18] H. Ries, G. Mank, J. Drexler, R. Heil, K. Huber, U. Kneissl, R. Ratzek, H. Ströher, T. Weber, and W. Wilke, Phys. Rev. C **29**, 2346 (1984), and references therein.

[19] R. A. Anderl, M. V. Yester, and R. C. Morrison, Nucl. Phys. A **212**, 221 (1973).

[20] M. Antonio P. V. de Moraes, and Marilia F. Cesar, Phys. Scr. **47**, 519 (1993); Nucl. Instrum. Methods Phys. Res. Sec. A **277**, 467 (1989).

[21] A. Shapiro and W. F. Stubbins, Nucl. Sci. Eng. **45**, 47 (1971).

[22] A. S. Soldatov and G. N. Smirenkin, Sov. J. Nucl. Phys. **55**, 1757 (1992); Report INDC(CCP) **359**, 59 (1992).

[23] A. M. Khan and J. W. Knowles, Nucl. Phys. A **179**, 333 (1972).

[24] L. Katz, A. P. Baerg, and F. Brown, in *Proceedings of the Second International Atomic Energy Conference* (United Nations, Geneva, 1958), Vol. 15, p. 188.

[25] A. Manfredini, M. Muchnik, L. Fiore, C. Ramorino, H. G. De Carvalho, R. Bosch, and W. Wolfli, Nuovo Cimento B **44**, 218 (1966).

[26] R. Bergere, H. Beil, B. Carlos, A. Veyssiere, and A. Lepretre, in *Proceedings of the International Conference on Nuclear Structure Studies Using Electron Scattering and Photoreaction, Sendai*, edited by K. Shoda and H. Ui (Japan, 1972).

[27] P. A. Dickey and P. Axel, Phys. Rev. Lett. **35**, 501 (1975).

[28] J. D. T. Arruda Neto, S. B. Herdade, B. S. Bhandari, and I. C. Nascimento, Phys. Rev. C **14**, 1499 (1976).

[29] I. S. Koretskaya, V. L. Kuznetsov, L. E. Lazareva, V. G. Nedoresov, and N. V. Nikitina, Sov. J. Nucl. Phys. **30**, 472 (1979).

[30] www.nndc.bnl.gov.

[31] http://www-nds.iaea.org.

[32] Krishichayan, M. Bhike, S. W. Finch, C. R. Howell, A. P. Tonchev, and W. Tornow, Nucl. Instrum. Methods Phys. Res. Sec. A **854**, 40 (2017).

[33] H. R. Weller, M. H. Ahmed, H. Gao, W. Tornow, Y. K. Wu, M. Gai, and R. Miskimen, Prog. Part. Nucl. Phys. **62**, 257 (2009).

[34] C. Bhatia, B. Fallin, M. E. Gooden, C. R. Howell, J. H. Kelley, W. Tornow, C. W. Arnold, E. M. Bond, T. A. Bredeweg, M. M. Fowler, W. A. Moody, R. S. Rundberg, G. Rusev, D. J. Vieira, J. B. Wilhelmy, J. A. Becker, R. Macri, C. Ryan, S. A. Sheets, M. A. Stoyer, and A. P. Tonchev, Nucl. Instrum. Methods Phys. Res. Sec. A **757**, 7 (2013).

[35] M. E. Gooden, C. W. Arnold, J. A. Becker, C. Bhatia, M. Bhike, E. M. Bond, T. A. Bredeweg, B. Fallin, M. M. Fowler, C. R. Howell, J. H. Kelley, Krishichayan, R. Marci, G. Rusev, C. Ryan, S. A. Sheets, M. A. Stoyer, A. P. Tonchev, W. Tornow, D. J. Vieira, and J. B. Wilhelmy, Nucl. Data Sheets **131**, 319 (2016).

[36] www.canberra.com.

[37] Changchun Sun, Ph.D. thesis, Duke University, 2009.

[38] A. P. Tonchev, S. L. Hammond, C. R. Howell, C. Huibregtse, A. Hutcheson, J. H. kelley, E. Kwan, R. Raut, G. Rusev, W. Tornow, T. Kawano, D. J. Vieira, and J. B. Wilhelmy, Phys. Rev. C **82**, 054620 (2010).

[39] V. V. Varlamov and N. N. Peskov, Report MSU-INP-2007-8/829, 2007; V. V. Varlamov, N. G. Efimkin, V. V. Surgutanov, A. A. Khoronenko, and A. P. Chernyaev, Book: Fotojad. Dannye, Moscow, 1987, http://www.nndc.bnl.gov/exfor/servlet/X4sGetSubent?reqx=82746&subID=220722011.

[40] Krishichayan, M. Bhike, A. P. Tonchev, and W. Tornow, EPJ Web Conf. **146**, 04018 (2017).

[41] M. Bhike, W. Tornow, Krishichayan, and A. P. Tonchev, Phys. Rev. C **95**, 024608 (2017).

[42] F. Tovesson, A. Laptev, and T. S. Hill, J. Nucl. Sci. Eng. **178**, 57 (2014).

[43] F. Tovesson and T. S. Hill, J. Nucl. Sci. Eng. **165**, 224 (2010).

[44] O. Shcherbakov, A. Donets, A. Evdokimov, A. Fomichev, T. Fukahori, A. Hasegawa, A. Laptev, V. Maslov, G. Petrov, Yu. Tuboltsev, and A. Vorobiev, J. Nucl. Sci. Technol. **39**, 230 (2002).